Available online at www.sciencedirect.com
SCIENCE DIRECT®
Journal of volcanology and geothermal research
ELSEVIER
Journal of Volcanology and Geothermal Research xx (2005) xxx–xxx
www.elsevier.com/locate/jvolgeores

Transient two-dimensional dynamics in the upper conduit of a rhyolitic eruption: A comparison of closure models for the granular stress

J. Dufek*, G.W. Bergantz

Department of Earth and Space Sciences, Box 351310, The University of Washington, Seattle, WA 98195, USA

Received 20 December 2003; accepted 1 September 2004

Abstract

To elucidate the role of particle collisions in redistributing momentum after fragmentation, a numerical study was performed comparing the behavior of an inviscid, or collision-less, granular material with a granular material whose viscosity and pressure were modeled using kinetic theory. The granular viscosity calculation is sensitive to particle size and three particle sizes were considered: .0002 m, .002 m, and .02 m. A critical volume fraction of gas (.75) identifies the onset of fragmentation, dividing the region of rhyolitic magma with dispersed bubbles from the region of turbulent gas with dispersed particles.

The transient simulations can be divided into two dynamic regimes: an initial shock followed by a transition to steady state. During the initial shock phase, treatment of the granular pressure and viscosity led to greater particle velocities relative to the inviscid calculation due to the development of higher gas pressure at fragmentation. However, as steady state is approached the viscosity slows the particle phase relative to the inviscid counterpart for particles greater than a millimeter. The modeled sub-millimeter particle velocity was insensitive to the treatment of the granular pressure and viscosity. Centimeter-scale particles have a much higher granular viscosity (up to 10^{-1} Pa · s) and the kinetic theory calculation is thus relevant in these conditions. After reaching steady state, the differential velocity between gas and particles at the conduit exit correlates with particle size for both the inviscid and granular viscosity calculations: negligible differential velocity develops for sub-millimeter particles, but centimeter-scale particles exit the conduit with >5% differential velocity between phases.

Keywords: volcanism; magma; explosive eruptions; two-phase flow

1. Introduction

The combination of high viscosity and high volatile contents in rhyolitic magmas contributes to the generation of some of the most explosive, Plinian-style eruptions (Carey and Sigurdsson, 1989). The

* Corresponding author.
E-mail address: dufek@u.washington.edu (J. Dufek).

0377-0273/$ - see front matter © 2005 Elsevier B.V. All rights reserved.
doi:10.1016/j.jvolgeores.2004.09.013

eruption sequence of depressurization, vesiculation, and fragmentation is often generalized to the setting of a high aspect-ratio conduit. This geometry is based upon the observation of relatively stationary central vents often associated with this class of eruption (Dobran, 1992, 1993; Slezin, 2003).

Two distinct regions of multiphase flow exist in a developing conduit eruption and are separated by a fragmentation front: magma/bubble flow and gas/particle flow (Fig. 1). Regions of the conduit that have become supersaturated in a volatile species in response to rapid depressurization will begin to form and grow bubbles. The high viscosity of the rhyolitic magma inhibits the formation of significant differential velocities between these phases, provided a permeable network of interconnected bubbles has not formed (Melnik et al., 2003). However, the net buoyancy force of the bubbles accelerates the magma/bubble flow. Thus the continuous depressurization during the rise of the magma provides a positive feedback as the bubbles continue to grow,

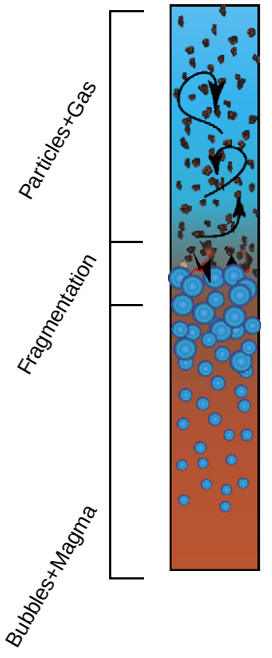

Fig. 1. Schematic representation of multiphase regions of the conduit: Below the fragmentation level the continuous phase is a rhyolitic magma with dispersed bubbles. At the critical gas fraction of .75 fragmentation occurs, creating a turbulent gas phase with dispersed particles.

and the magma/bubble mixtures accelerates until reaching fragmentation.

The precise mechanism of fragmentation remains poorly understood with little unambiguous data to differentiate between ductile and brittle mechanisms (Dingwell, 1996; Mader, 1998). Sparks (1978) initially suggested that fragmentation is associated with .75 gas volume fraction, due to many observations of vesicularity in this range and due to the close correspondence of this value with the maximum packing limit of spheres of a single diameter. Observations of much lower vesicularity (Bachmann et al., 2000; Thomas et al., 1994) in some silicic pumices motivates further scrutiny of the fragmentation limit. It has been proposed that there is a correlation between vesicularity and viscosity of the host magma, with more viscous magma fragmenting at lower gas volume fraction (Gardner et al., 1996; Papale, 1999). However, we treat fragmentation by a static model assuming that it occurs at a gas volume fraction of .75. This facilitates comparison of the granular stress differences by reducing the degrees of freedom in the study; a dynamic fragmentation model will be the subject of future studies.

Following fragmentation the multiphase mixture consists of a turbulent gas with dispersed particles or melt droplets. Two principle interactions are responsible for the redistribution of momentum in this regime: particle–particle interaction and particle–gas interaction. Particles transmit momentum to each other directly through either elastic or inelastic collisions. Particle–fluid interaction occurs chiefly as a result of the drag force between a particle and the fluid when the two are moving relative to each other.

The aerodynamic response time of a particle is the characteristic timescale by which a particle responds to these changes in the flow field. This timescale can be developed by considering the equation of motion for the particle in a fluid. For situations in which the density of the particle is much greater than the density of the fluid, such as in the gas/particle flow following fragmentation, and neglecting particle collisions, gravity and wall interaction, the equation of motion for a particle with small particle Reynolds number reduces to (Maxey and Riley, 1983):

$$\frac{\mathrm{d}\mathbf{c}_i^{\mathrm{s}}}{\mathrm{d}t} = \frac{-6\pi d_{\mathrm{p}}\mu_{\mathrm{g}}}{m_{\mathrm{p}}}\left(\mathbf{c}_i^{\mathrm{s}} - \mathbf{c}_i^{\mathrm{g}}\right), \tag{1}$$

where $\mathbf{c}_i^s$ is the instantaneous velocity of the particle, $\mathbf{c}_i^g$ is the instantaneous velocity of the gas, μ_g is the gas viscosity, m_p is the mass of the particle, and d_p is the particle diameter. (The decomposition of the instantaneous velocity into an average and fluxuating component will be used throughout the paper, $\mathbf{c}_i=\langle\mathbf{c}_i\rangle+\mathbf{C}_i=\mathbf{u}_i+\mathbf{C}_i$. A list of all symbols used is included in the Appendix A.) For a given differential velocity between the particle and the gas, the timescale by which the particle accelerates to match the velocity of the gas is given by the reciprocal of the leading coefficients on the right-hand side of Eq. (1). Rearrangement so that this timescale is expressed in terms of the particle density yields:

$$t_p = \frac{\rho_p d_p^2}{6\pi\mu_g}. \tag{2}$$

If the density of the particle and the viscosity of the gas remains constant, then the aerodynamic response timescale increases as the square of the particle diameter. The ratio of the aerodynamic timescale to the characteristic timescale of the gas motion is typically referred to as the Stokes number (Eaton and Fessler, 1994). Larger Stokes number particles are slow to respond to gas motion whereas small Stokes number particles behave as tracers to the fluid motion.

The calculation of numerous individual particle paths along with a turbulent flow field is computationally intractable. Hence, work in both the volcanological and industrial community has aimed to try to develop better constitutive models to predict the macroscopic manifestations of the particle–particle and particle–fluid interactions (Dobran, 1992; Gidaspow, 1994; Lun et al., 1984).

In the context of conduit flow, two multiphase theories have been applied: homogenous (single-fluid simulations) and non-homogenous (multi-fluid simulations). Homogeneous conduit flow models (Wilson and Head, 1981) average the phase properties to create one effective fluid with bulk properties such as density. The particle–particle and particle–fluid interactions are approximated through the designation of a viscosity to relate stress to strain rates in the bulk material. The implicit assumption in these models is that the aerodynamic timescale of the dispersed phase is close to zero. This assumption applies well for bubble/rhyolitic magma flow with low permeability, because there is little relative velocity between phases (Mader, 1998). Above the level of fragmentation a homogenous model should perform well provided that the particles remain tracers of all scales of fluid motion (Dobran, 2001), i.e. the particle size is small enough that the Stokes number approaches zero for any given eddy size.

However, Dobran (1992) demonstrated that significant mechanical non-equilibrium effects (differential velocities between phases) are important in viscous conduit flow, and developed a one-dimensional, steady state, two-phase flow model. This model has been subsequently modified for different magma viscosity relationships accounting for variable magma composition and crystal content (Papale and Dobran, 1994; Papale et al., 1998), different volatile effects (water and carbon dioxide; Papale and Polacci, 1999), different fragmentation criteria (Papale, 1999), and fragmentation efficiency (Papale, 2001). These models have produced results consistent with quasi steady state behavior of Mt. St. Helens and Vesuvius (Papale and Dobran, 1994).

Previous non-homogeneous multi-fluid numerical simulations (Dobran, 1992; Papale and Dobran, 1994) have treated the particle phase as inviscid. That is, in one-dimensional simulations where viscosity appears in the drag relations, the particle-wall drag is set to zero. However, the viscosity of the gas is adjusted using mixture theory to account for the distortion of the flow field created by the particles and the apparent increase in viscosity that this creates (Dobran, 1992). Papale (2001) modified this model by introducing a parameterized normal collisional stress (analogous to the granular pressure described here) that provided a repulsive force for high particle concentrations and viscosity for the system was developed using mixture theory.

The inviscid granular phase assumption is appropriate in regions of the flow where there is no collisional redistribution of momentum, or in a fully fluidized bed far from boundaries (Gidaspow, 1994; Appendix B). However, the magnitude of collisional redistribution of momentum following fragmentation remains an open question. All the phases in a multiphase system are coupled to each other through

drag force relationships, and consequently changes in the constitutive relations of one phase affects the other phases. This, in turn, may result in counter-intuitive feedback in the conduit system. In order to examine the effect of particle collisions in the conduit, a suite of numerical simulations were performed in which the constitutive equation for the granular phase was varied to reflect the collisional and collision-less counterparts. Our approach differs from that of Papale (2001) in that the terms of the granular stress tensor are developed using kinetic theory with the granular viscosity and pressure linked to the local velocity field of the particles through the granular temperature.

2. Multi-fluid model for multiphase flow

2.1. Multi-fluid theory

Our parameterization study of the granular constitutive relationship was performed in the context of a transient, 2-D, isothermal, multi-fluid simulation of conduit dynamics. The multi-fluid treatment of multiphase phenomena has been implemented in a range of volcanological and industrial problems (Dobran et al., 1993; Gidaspow, 1986; Neri et al., 2002; Neri and Macedonio, 1996). The multi-fluid methodology treats each phase as a separate continuum with differential velocities between phases. The particle phase(s) are averaged to form continuum conservation equations. The 'true' fluid and particle fluids are interpenetrating continua; that is, the volume fraction of each phase is calculated at individual grid points. The sum of the volume fractions at any one point is required to be unity:

$$\varepsilon_g + \varepsilon_s = 1. \tag{3}$$

Additionally, the conservation equations for the different fluids are:

Below the level of fragmentation

Continuity:

$$\frac{\partial}{\partial t}\left(\varepsilon_g \rho_g\right) + \frac{\partial}{\partial \mathbf{x}_i}\left(\varepsilon_g \rho_g \mathbf{u}_i^g\right) = R_g, \quad \text{gas} \tag{4}$$

$$\frac{\partial}{\partial t}\left(\varepsilon_m \rho_m\right) + \frac{\partial}{\partial \mathbf{x}_i}\left(\varepsilon_m \rho_m \mathbf{u}_i^m\right) = R_m, \quad \text{magma} \tag{5}$$

Conservation of momentum:

$$\frac{\partial}{\partial t}\left(\varepsilon_g \rho_g \mathbf{u}_i^g\right) + \frac{\partial}{\partial \mathbf{x}_j}\left(\varepsilon_g \rho_g \mathbf{u}_i^g \mathbf{u}_j^g\right) = \frac{\partial}{\partial \mathbf{x}_j}\left(\mathbf{S}_{ij}^g\right) + \varepsilon_g \rho_g \mathbf{g} - \mathbf{I}_j^{gm}, \quad \text{gas} \tag{6}$$

$$\frac{\partial}{\partial t}\left(\varepsilon_m \rho_m \mathbf{u}_i^m\right) + \frac{\partial}{\partial \mathbf{x}_j}\left(\varepsilon_m \rho_m \mathbf{u}_i^m \mathbf{u}_j^m\right) = \frac{\partial}{\partial \mathbf{x}_j}\left(\mathbf{S}_{ij}^m\right) + \varepsilon_m \rho_m \mathbf{g} + \mathbf{I}_j^{gm}, \quad \text{magma} \tag{7}$$

Above the level of fragmentation

Continuity:

$$\frac{\partial}{\partial t}\left(\varepsilon_g \rho_g\right) + \frac{\partial}{\partial \mathbf{x}_i}\left(\varepsilon_g \rho_g \mathbf{u}_i^g\right) = 0, \quad \text{gas} \tag{8}$$

$$\frac{\partial}{\partial t}\left(\varepsilon_p \rho_p\right) + \frac{\partial}{\partial \mathbf{x}_i}\left(\varepsilon_p \rho_p \mathbf{u}_i^p\right) = 0, \quad \text{particles} \tag{9}$$

Conservation of momentum:

$$\frac{\partial}{\partial t}\left(\varepsilon_g \rho_g \mathbf{u}_i^g\right) + \frac{\partial}{\partial \mathbf{x}_j}\left(\varepsilon_g \rho_g \mathbf{u}_i^g \mathbf{u}_j^g\right) = \frac{\partial}{\partial \mathbf{x}_j}\left(\mathbf{S}_{ij}^g\right) + \varepsilon_g \rho_g g - \mathbf{I}_j^{gp}, \quad \text{gas} \tag{10}$$

$$\frac{\partial}{\partial t}\left(\varepsilon_p \rho_p \mathbf{u}_i^p\right) + \frac{\partial}{\partial \mathbf{x}_j}\left(\varepsilon_p \rho_p \mathbf{u}_i^p \mathbf{u}_j^p\right) = \frac{\partial}{\partial \mathbf{x}_j}\left(\mathbf{S}_{ij}^p\right) + \varepsilon_p \rho_p g + \mathbf{I}_j^{gp}, \quad \text{particles} \tag{11}$$

Here ε is the volume fraction of either particles, magma, or gas, $\mathbf{S}_{ij}$ are the stress tensors, $\mathbf{I}_j$ are the inter-phase momentum transfer terms, and R are the exsolution rates for the magmatic case (Jackson, 1983; Syamlal, 1987). The subscript (g) refers to the gas phase, (m) refers to the magma below fragmentation, and (p) to the particles above fragmentation.

2.2. Constitutive relations below the level of fragmentation

The magmatic stress tensor, $\mathbf{S}_{ij}^{\mathrm{m}}$, is given by:

$$\mathbf{S}_{ij}^{\mathrm{m}} = -P_{\mathrm{m}}\boldsymbol{\delta}_{ij} + \boldsymbol{\tau}_{ij}^{\mathrm{m}}, \tag{12}$$

where P_{m} is the pressure and $\boldsymbol{\tau}_{ij}^{\mathrm{m}}$ is the deviatoric component of the magmatic stress tensor. The gas and magmatic pressure are assumed to be equivalent for these calculations (Papale and Dobran, 1994). The deviatoric component is closed using the experimental compilation of Hess and Dingwell (1996) for the viscosity of hydrous leucogranitic melt:

$$\mathbf{s}_{ij}^{\mathrm{m}} = 2\mu_{\mathrm{m}}\varepsilon_{\mathrm{m}}\mathbf{D}_{ij}^{\mathrm{m}}, \tag{13}$$

where:

$$\log(\mu_{\mathrm{m}}) = [-3.545 + .833\ln(w)] + [9601 - 2368\ln(w)] / \{T - [195.7 + 32.25\ln(w)]\}, \tag{14}$$

where w is the weight percent of water, and T is the temperature in Kelvin. The density of the magma is held constant at 2300 kg/m^3. The viscosity of the gas phase is held constant at 5.0×10^{-5} Pa·s, and its density derived from the ideal gas relation both below and above the fragmentation front. As a first approximation, no turbulent viscosity model was used in these simulations. The simulations of Agrawal et al. (2001) suggest that provided $\rho_{\mathrm{p}}\varepsilon_{\mathrm{s}} \gg \rho_{\mathrm{g}}\varepsilon_{\mathrm{g}}$ riser dynamics are relatively insensitive to the use of a turbulence model. This condition is satisfied in most of the computational domain for this problem, although further investigation of turbulence models in this parameter space is needed.

Below the level of fragmentation, it is assumed that the high viscosity of the magma will inhibit large velocity differences between the bubbles and the magma. Hence a simple Stokes drag relation is used:

$$\mathbf{I}_i^{\mathrm{gm}} = \frac{6\pi\mu_{\mathrm{m}}}{\rho_{\mathrm{m}}d_{\mathrm{bub}}^2}\left(\mathbf{u}_i^{\mathrm{g}} - \mathbf{u}_i^{\mathrm{m}}\right) - \varepsilon_{\mathrm{g}}\frac{\partial}{\partial \mathbf{x}_i}P_{\mathrm{g}} + R_{\mathrm{g}}\mathbf{u}_i^{\mathrm{m}}. \tag{15}$$

The first term is the Stokes drag term and the second is the buoyancy term. The last term accounts for the mass transfer from the magma to the bubbles. In Eq. (15) the bubbles are assumed spherical and non-deforming.

2.2.1. Volatile exsolution model

The equilibrium solubility of water has been modeled as:

$$C_{\mathrm{eq}} = P_{\mathrm{g}}^{.5}\left(0.4874 - \frac{608.0}{T} + \frac{489530}{T^2}\right) + P_{\mathrm{g}}\left(-0.06062 + \frac{135.6}{T} - \frac{69200}{T^2}\right) + P_{\mathrm{g}}^{1.5}\left(0.00253 - \frac{4.154}{T} + \frac{1509.0}{T^2}\right) \tag{16}$$

[The equation is reparameterized and simplified from the solubility model of Zhang (1999) by Y. Zhang.] P_{g} is the gas pressure in MPa, T is the temperature in Kelvin, and C_{eq} is the equilibrium solubility in weight percent (Zhang, 1999). Immediately following depressurization the dissolved water content will be greater than the equilibrium dissolved water content for the lower pressure state. This super-saturation will drive bubble formation and growth. Water is the only volatile phase used here. While this is oversimplified compared with the natural case, it was considered adequate from the standpoint of comparing the dynamics of the granular viscosity phase versus an inviscid granular phase.

Bubble nucleation and growth is considered almost instantaneous upon super-saturation. This is also a simplification, as bubble growth has been demonstrated to be primarily diffusion controlled and some time is required to diffuse water from the melt into the bubbles (Lyakhovsky et al., 1996). Subtracting the equilibrium solubility from the initial dissolved water content gives the weight percent of water exsolved. This can then be converted to the volume fraction of exsolved water through the equation of state. In practice, this was accomplished by setting the reaction rates in Eqs. (4) and (5) such that the exsolution of supersaturated water was accomplished over the duration of one time-step, which for these simulations was on the order of 1.0×10^{-4} s.

$$R_{\mathrm{g}} = \Delta V_{\mathrm{g}}\rho_{\mathrm{g}}/\Delta t, \tag{17}$$

and

$$R_{\mathrm{s}} = -\Delta V_{\mathrm{g}}\rho_{\mathrm{g}}/\Delta t, \tag{18}$$

where ΔV_g is the volume fraction of gas exsolved in one time step.

The volume fraction of exsolved gas can also be converted into an effective bubble diameter using the prescribed bubble number density, 10^{15} m^{-3} based upon the experiments of Hurwitz and Navon (1994). The bubble diameter d_{bub} is needed to compute the interphase drag between the bubbles and the magma (Eq. (15)).

2.3. Constitutive relations for the granular material: kinetic theory

The binary collision of particles represents a possible means of redistributing momentum in a particle dense region following fragmentation. On macroscopic scales this momentum diffusivity can be modeled using a granular viscosity to close the deviatoric component of the granular stress–strain rate relationship, and a granular pressure for the isotropic component (Lun et al., 1984; Syamlal, 1987). To develop the properties of the collisional regime, kinetic theory, very similar to that used in the estimation of gas viscosities from molecular collisions, is employed (Gidaspow, 1994). Lun et al. (1984) and Syamlal (1987) developed the method implemented in these calculations, and the reader is referred to these sources for a more detailed accounting of the procedure. The following set of equations results from their analysis considering binary, inelastic collisions of particles:

$$\mathbf{S}^{\mathrm{p}}_{ij} = -P_{\mathrm{p}}\boldsymbol{\delta}_{ij} + \boldsymbol{\tau}^{\mathrm{p}}_{ij}, \tag{19}$$

where $\mathbf{S}^{\mathrm{p}}_{ij}$ is the granular stress tensor, P_{p} is the granular pressure, and $\boldsymbol{\tau}^{\mathrm{p}}_{ij}$ is the viscous stress tensor. The granular pressure is given by:

$$P_{\mathrm{p}} = 2(1+e)\rho_{\mathrm{p}} g_0 \varepsilon_{\mathrm{p}}^2 \theta_{\mathrm{p}}, \tag{20}$$

and the granular viscous stress tensor is given by:

$$\boldsymbol{\tau}^{\mathrm{p}}_{ij} = 2\mu_{\mathrm{p}}\mathbf{D}^{\mathrm{p}}_{ij} + \lambda_{\mathrm{p}}\mathbf{D}^{\mathrm{p}}_{ii}\boldsymbol{\delta} ij. \tag{21}$$

Here $\mathbf{D}^{\mathrm{p}}_{ij}$ is the rate of strain tensor:

$$\mathbf{D}^{\mathrm{p}}_{ij} = \frac{1}{2}\left[\frac{\partial \mathbf{u}^{\mathrm{p}}_i}{\partial \mathbf{x}_j} + \frac{\partial \mathbf{u}^{\mathrm{p}}_j}{\partial \mathbf{x}_i}\right], \tag{22}$$

and g_0 is the radial distribution function (Lebowitz, 1964):

$$g_0 = \frac{1}{\varepsilon_{\mathrm{g}}} + \frac{3\varepsilon_{\mathrm{p}}}{2\varepsilon_{\mathrm{p}}^2}, \tag{23}$$

$\boldsymbol{\delta}_{ij}$ is the Kronecker delta, and the Einstein summation convention is applied for repeated indices. These relations are often cast in terms of the coefficient of bulk viscosity, which is defined as:

$$\xi_{\mathrm{p}} \equiv \lambda_{\mathrm{p}} + {}^{2}/_{3}\mu_{\mathrm{p}}. \tag{24}$$

The viscous stress tensor is composed of the second viscosity coefficient component (λ_{p}) and the shear viscosity component (μ_{p}):

$$\lambda_{\mathrm{p}} = d_{\mathrm{p}}\rho_{\mathrm{p}}\sqrt{\theta_{\mathrm{p}}}\varepsilon_{\mathrm{p}}\left[\frac{4(1+e)\varepsilon_{\mathrm{p}} g_0}{3\sqrt{\pi}} - \frac{\sqrt{\pi}}{9(3-e)} - \frac{2\sqrt{\pi}(1+e)(3e-1)\varepsilon_{\mathrm{p}} g_0}{45(3-e)} - \frac{8\varepsilon_{\mathrm{p}} g_0(1+e)}{15\sqrt{\pi}}\right], \tag{25}$$

$$\mu_{\mathrm{p}} = \frac{d_{\mathrm{p}}\rho_{\mathrm{p}}\sqrt{\theta_{\mathrm{p}}}}{2}\varepsilon_{\mathrm{p}}\left[\frac{\sqrt{\pi}}{3(3-e)} + \frac{2\sqrt{\pi}(1+e)(3e-1)\varepsilon_{\mathrm{p}} g_0}{15(3-e)} + \frac{8\varepsilon_{\mathrm{p}} g_0(1+e)}{5\sqrt{\pi}}\right]. \tag{26}$$

An important parameter in these calculations is the granular temperature (θ_{p}). It is a measure of the fluctuating component of the particle velocity and is defined as

$$\theta_{\mathrm{p}} \equiv \frac{1}{3}\langle \mathbf{C}^{\mathrm{p}}_i \mathbf{C}^{\mathrm{p}}_i \rangle \tag{27}$$

Here the instantaneous velocity ($\mathbf{c}^{\mathrm{p}}_i$) for the solid phase has been decomposed into the average velocity or 'hydrodynamic' velocity $\mathbf{u}^{\mathrm{p}}_i$ and a fluctuating component $\mathbf{C}^{\mathrm{p}}_i$. The averaging method, $\langle\rangle$, is defined in the Appendix B. To solve for the granular temperature a transport equation for the granular energy must be developed similar to the momentum equation above. An algebraic approximation was developed by Syamlal (1987) and is used in these calculations:

$$\theta_{\mathrm{p}} = \left\{\frac{-K_1\varepsilon_{\mathrm{p}}\mathbf{D}^{\mathrm{p}}_{ii} + \sqrt{\left(K_1\mathbf{D}^{\mathrm{p}}_{ii}\varepsilon_{\mathrm{p}}\right)^2 + 4K_4\varepsilon_{\mathrm{p}}\left[K_2(\mathbf{D}^{\mathrm{p}}_{ii})^2 + 2K_3(\mathbf{D}^{\mathrm{p}}_{ii})^2\right]}}{2\varepsilon_{\mathrm{p}}K_4}\right\}^2 \tag{28}$$

where:

$$K_1 = 2(1+e)\rho_{\mathrm{p}} g_0, \tag{29}$$

$$K_2 = \frac{4 d_p \rho_p (1+e)\varepsilon_p g_0}{3\sqrt{\pi}} - \frac{2}{3} K_3, \tag{30}$$

$$K_3 = \frac{d_p \rho_p}{2}\left[\frac{\sqrt{\pi}}{3(3-e)}\left(1 + .4(1+e)(3e-1)\varepsilon_p g_0\right) + \frac{8\varepsilon_p g_0 (1+e)}{5\sqrt{\pi}}\right], \tag{31}$$

$$K_4 = \frac{12(1-e^2)\rho_p g_0}{d_p \sqrt{\pi}} \tag{32}$$

This equation assumes that the granular energy is dissipated locally, and is most appropriate for fully developed, simple shear flows (Gidaspow, 1994; Syamlal, 1987). Non-steady forcing in the conduit may give rise to advective transport of granular energy that is not treated with this assumption.

The expression for the granular stress shown above is complex but some intuition can be gained from examining a simpler, non-rigorous treatment as demonstrated by Gidaspow (1994). Assuming a Taylor expansion can be performed, the momentum flux yields the expression:

$$\mathbf{M}(x+1)\langle \mathbf{c} \rangle = \mathbf{M}(x)\langle \mathbf{c} \rangle + l\langle \mathbf{c} \rangle \frac{d\mathbf{M}}{d\mathbf{x}}, \tag{33}$$

where

$$\mathbf{M} = (m\mathbf{c}). \tag{34}$$

Here l is the mean free path. Gidaspow (1994) assumes in this simple case that the particle velocity distribution is Maxwellian. That is, the particle velocities vary randomly around a mean velocity. Rearrangement, assuming constant density, and using the observation that the change in momentum flux equals the product of a viscosity and the strain rate yields the expression:

$$\mu = l\rho\langle \mathbf{c} \rangle, \tag{35}$$

or that the viscosity is simply the product of the mean free path, the density, and the average velocity. Using the Maxwellian distribution to determine the average velocity, this expression yields:

$$\mu = \left(\frac{1}{3\sqrt{\pi}}\right)\rho_p d_p \sqrt{\theta_p}. \tag{36}$$

In both the expression of Lun et al. (1984) and in the simplified Gidaspow (1994) example, the granular viscosity is proportional to the square root of the granular temperature and diameter of the particle, and motivates the examination of the different particle sizes in this study.

Another parameter is the restitution coefficient (e), which is a measure of the inelasticity of particle collisions (e=1 is for a perfectly elastic collision). In general, the coefficient of restitution is a function of the material and velocity of collision, with higher velocity impacts having lower coefficients of restitution (Johnson, 1985). It is difficult to parameterize the restitution coefficient for pumice and droplet materials. In this study a value of .8 was used and a sensitivity analysis is presented below.

For the particle–gas momentum transfer above the level of fragmentation the relation of Syamlal et al.

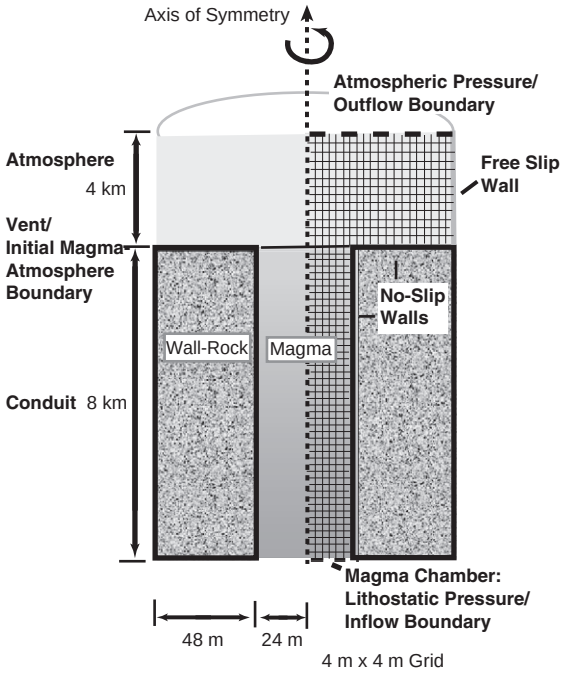

Fig. 2. Schematic representation of the conduit model: The bottom boundary is specified as the lithostatic pressure at a depth of 8 km. Sidewalls are assumed to be no-slip and the cross-sectional area expands at the vent to permit choked flow. An outflow boundary condition is specified 4 km above the vent. The modeled conduit region is 8 km high and 24 m in radius. Symmetry is assumed about the centerline. The numerical grid is regular (square) and resolution is 4 m×4 m. This schematic is horizontally exaggerated ~100:1.

(1993) was used which is based on correlations from terminal velocity measurements:

$$\mathbf{I}_i^{\mathrm{gp}} = \frac{3\varepsilon_{\mathrm{p}}\varepsilon_{\mathrm{g}}\rho_{\mathrm{g}}}{4V_{\mathrm{r}}d_{\mathrm{p}}} C_{\mathrm{D}}^{\mathrm{s}} |\mathbf{u}_i^{\mathrm{g}} - \mathbf{u}_i^{\mathrm{p}}| (\mathbf{u}_i^{\mathrm{g}} - \mathbf{u}_i^{\mathrm{p}}) - \varepsilon_{\mathrm{p}} \frac{\partial}{\partial \mathbf{x}_i} P_{\mathrm{g}}, \tag{37}$$

where V_{r} is the terminal velocity correlation (the ratio of the terminal velocity of a group of particles to that of a single, isolated particle) given by the expression:

$$V_{\mathrm{r}} = .5\left(A - .06Re_{\mathrm{p}}\right) + \sqrt{\left(.06Re_{\mathrm{p}}\right)^2 + .12Re_{\mathrm{p}}(2B - A) + A^2}. \tag{38}$$

In this relation,

$$A = \varepsilon_{\mathrm{g}}^{4.14}, \tag{39}$$

$$B = \begin{cases} .8\varepsilon_{\mathrm{g}}^{1.28} & \text{if } \varepsilon_{\mathrm{g}} \leq .85 \\ \varepsilon_{\mathrm{g}}^{2.65} & \text{if } \varepsilon_{\mathrm{g}} > .85 \end{cases}. \tag{40}$$

The single-sphere drag function and particle Reynolds number are given by:

$$C_{\mathrm{D}}^{\mathrm{s}} = \left[.63 + \frac{4.8}{\sqrt{Re}}\right]^2, \tag{41}$$

and

$$Re_{\mathrm{p}} = \frac{d_{\mathrm{p}}|\mathbf{u}_{\mathrm{s}} - \mathbf{u}_{\mathrm{g}}|\rho_{\mathrm{g}}}{\mu_{\mathrm{g}}}. \tag{42}$$

2.4. Conduit parameters

Conduit flow requires that a large region of the conduit be represented in the model even though the phenomena of interest to this study are isolated to the post-fragmentation region. This requirement arises because the behavior at fragmentation is altered by conditions deeper in the conduit such as mass-flux and pressure. The idealized conduit geometry is depicted schematically in Fig. 2 and is 24 m in radius and 8 km from base to vent. Symmetry about the centerline is assumed. At the bottom boundary the pressure is fixed at the lithostatic pressure at a depth of 8 km (~212 MPa assuming a crustal density of 2700 kg/m^3). At the

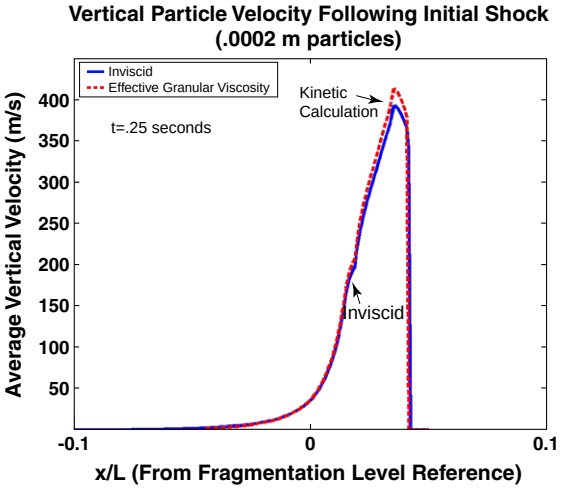

Fig. 3. Particle velocity following initial shock (~.25 s after start of simulation): Dashed line refers to particle velocity where the effective granular stress tensor has been computed using kinetic theory, and the solid line denotes the particle velocity in a simulation using an inviscid granular material. Both curves refer to simulations with .0002 m diameter particles. The length axis has been non-dimensionalized by dividing by the conduit length and is referenced to 0.0 at the point of fragmentation.

Table 1
Summary of conditions in the upper conduit at steady state[a]

Simulation name	d_{p} (m)	S_{ij}	$u_{\mathrm{g}}^{\mathrm{exit,max}}$ (m/s)	$u_{\mathrm{g}}^{\mathrm{exit,avg}}$ (m/s)	$u_{\mathrm{p}}^{\mathrm{exit,ma}}$ (m/s)	$u_{\mathrm{p}}^{\mathrm{exit,avg}}$ (m/s)	$P_{\mathrm{g}}^{\mathrm{exit}}$ (Pa)	$\mu_{\mathrm{p}}^{\mathrm{max}}$ (Pa s)	Mass-Flux (kg/m^3 s)	D_{F} (m)
I (Viscosity)	.0002	C	220.5	206.5	220.5	205.5	2.23×10^{6}	2.52×10^{-5}	3.66×10^{7}	1620
II (Viscosity)	.002	C	194.5	166.2	188.1	157.7	1.82×10^{6}	1.45×10^{-3}	3.09×10^{7}	1440
III (Viscosity)	.02	C	172.6	145.1	162.5	137.8	1.60×10^{6}	1.36×10^{-1}	3.04×10^{7}	1280
I (Inviscid)	.0002	C-L	220.7	216.3	220.6	214.1	2.22×10^{6}	0.0	3.71×10^{7}	1576
II (Inviscid)	.002	C-L	204.8	195.1	197.2	185.3	1.80×10^{6}	0.0	3.63×10^{7}	1416
III (Inviscid)	.02	C-L	182.4	171.9	170.1	163.3	1.59×10^{6}	0.0	3.60×10^{7}	1256

[a] The conduit diameter is 24 m and the height is 8 km in all simulations. d_{p} is the particle diameter, S_{ij} is the granular stress tensor approximation used: C—collisional, C-L—collision-less, $u_{\mathrm{g}}^{\mathrm{exit,max}}$ and $u_{\mathrm{p}}^{\mathrm{exit,max}}$ are the exit gas and particle centerline velocities, respectively, $u_{\mathrm{g}}^{\mathrm{exit,avg}}$ and $u_{\mathrm{p}}^{\mathrm{exit,avg}}$ are the average exit gas and particle velocities, $P_{\mathrm{g}}^{\mathrm{exit}}$ is the exit pressure, $\mu_{\mathrm{s}}^{\mathrm{max}}$ is the maximum granular shear viscosity; the mass-flux is recorded at the vent, and D_{F} is the depth of fragmentation.

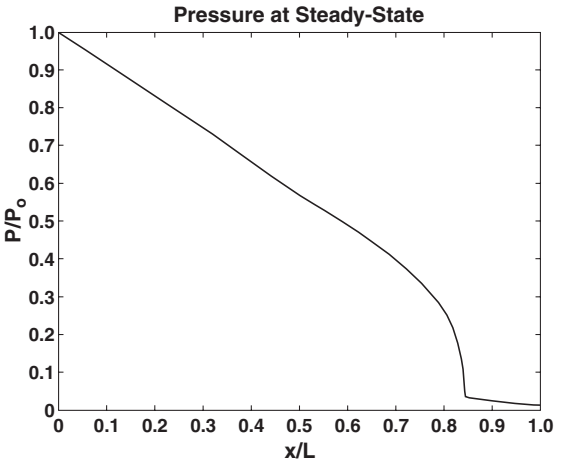

Fig. 4. Non-dimensionalized pressure at steady state: The pressure was normalized by the lithostatic pressure at 8 km depth and the height was normalized by the conduit length. Both the inviscid and effective granular viscosity calculations produce pressure greater than lithostatic below the fragmentation level.

top of the idealized vent the cross-sectional area increases to permit choked flow conditions. An outlet boundary at atmospheric pressure is specified 4 km above the vent. Sidewall boundaries were designated no-slip below the level of the conduit vent. All simulations were solved on a regular grid with numerical resolution of 4×4 m. Radial changes in the volume fraction of different phases through time can be examined in these two-dimensional simulations. However, the resolution and imposed symmetry at the center-channel may inhibit the development of meso-scale structures in these simulations (Agrawal et al., 2001; Neri and Gidaspow, 2000). The conduit was considered isothermal at 850 °C, and initial water concentration was assumed to be 4.5 wt.% water and is in rough agreement with the water concentration of many rhyolitic eruptions (Anderson et al., 1989). At the start of the simulations all the water is assumed to be dissolved in the magma and the pressure is magmastatic. Under natural conditions such an initial condition is unlikely because a significant component of gas would likely have already exsolved

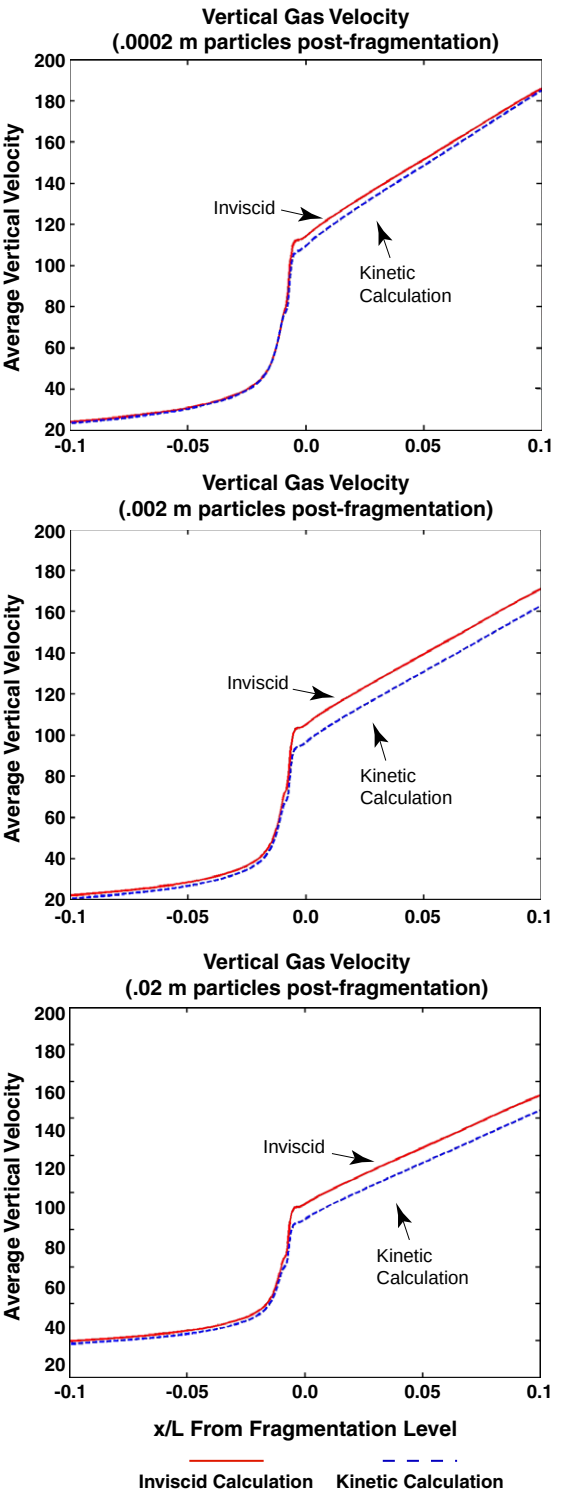

Fig. 5. Centerline gas velocities near the level of fragmentation: Gas velocities for both the inviscid (—) and granular effective viscosity (- - -) calculations are shown for the simulations using .0002 m, .002 m, and .02 m particles.

before reaching these depths. Hence, the details of the initial shock are probably unrealistic. However, these simulations proceed to a steady state quickly and this behavior will be examined in detail. Fragmentation is assumed to take place at the critical gas volume fraction of .75. Although the parameters selected for the numerical simulations shown below were chosen with guidance from natural constraints, we stress that this study does not aim to model a particular eruption, but rather to evaluate the sensitivity of the different granular constitutive relations in a general sense for rhyolitic eruptions.

2.5. Numerical treatment of the multi-fluid equations

The previous set of equations were solved using a modified form of the MFIX (Syamlal et al., 1993) multi-fluid code adapted for volcanic conduit conditions. The MFIX code uses an implicit multifield (IMF) finite difference solution procedure (Harlow and Amsden, 1975) developed for multiphase flow. This code was validated for the industrial fluidized bed application through comparison with experimental results (O'Brien and Syamlal, 1991). A switching function was incorporated to handle the magma/solid particle transition. Below the critical volume fraction the magmatic viscosity of Hess and Dingwell (1996) is applied. Above the level of fragmentation, in the atmosphere, the viscosity of the particle phase is either a.) calculated from kinetic theory or b.) assumed inviscid. The model was run on a single processor with a 18×3000 grid (4 m×4 m resolution). Small timesteps of ~1.0×10^{-4} s were required for convergence. The model was tested on a Beowulf multiprocessor system, but the geometry and node configuration of this problem scaled poorly.

3. Simulation results

Three different particle sizes (.0002 m, .002 m, and .02 m) were examined in order to compare the

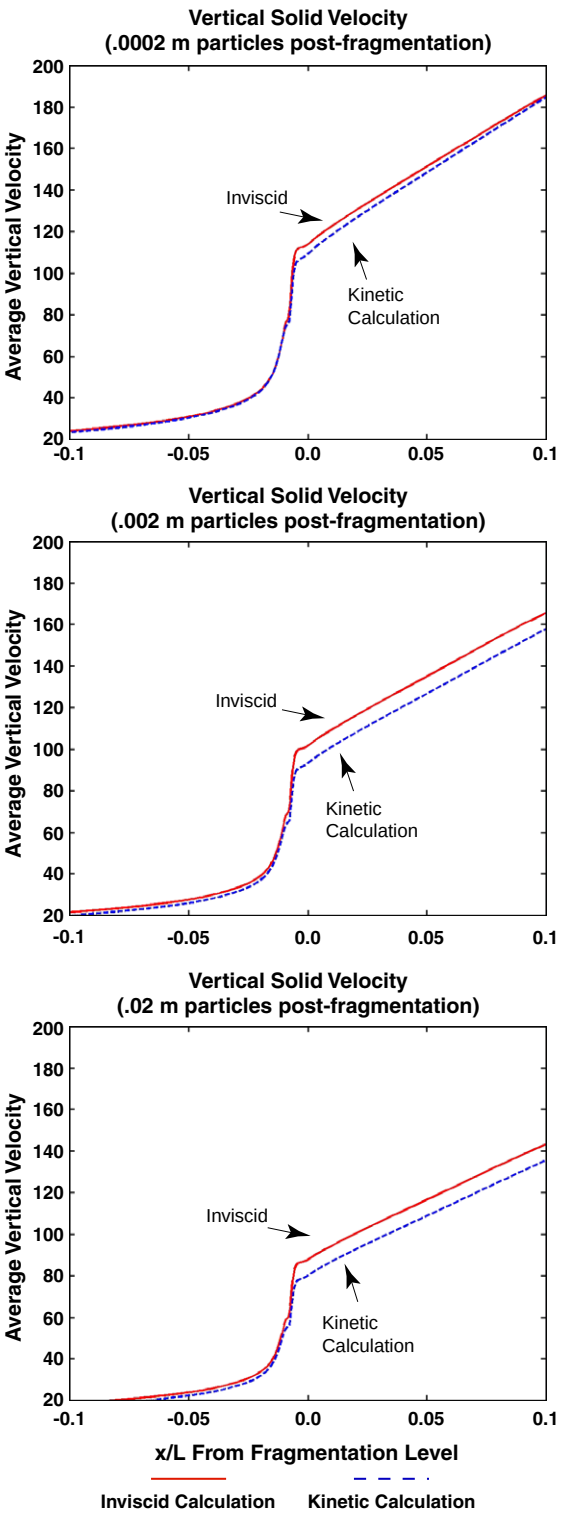

Fig. 6. Centerline magma and particle velocities near the level of fragmentation: Magma and particle velocities for both the inviscid (—) and granular effective viscosity (- - -) calculations are shown for the simulations using .0002 m, .002 m, and .02 m particles. Below the 0.0 point, the magmatic rheology applies, and above this level either kinetic theory or the inviscid assumption is applied.

collisional granular stress to the collision-less inviscid granular approximation. To reduce the degrees of freedom, all other variables were held constant between the simulations. Table 1 summarizes some of the relevant results.

3.1. Initial shock

Immediately following rapid depressurization of the magma, a shock develops that propagates up the conduit. An exsolution front propagates back into the conduit and the fragmentation zone develops. The velocity of the multiphase mixture immediately following the shock (both particles and gas) is slightly greater in the simulations using kinetic theory for the granular stress (Fig. 3). This pattern of greater velocities in the initial shock for the kinetic theory calculations was observed for the .0002 m, .002 m, and .02 m grain sizes. This is likely the result of the greater over-pressure that develops in these calculations in the initial stages of the eruption. As the simulation proceeds, a quasi-steady state pressure is approached that resembles similar results achieved through the calculations of Papale and Dobran (1994) with about 12% overpressure with respect to the lithostatic gradient immediately below the fragmentation level (Fig. 4). The velocity following the shock for the case of the .0002 m particles calculation was ~410 m/s (kinetic) and ~390 m/s (inviscid) above the level of the vent. These velocities, however, are not sustained and the steady state velocities are approximately half these values.

3.2. Quasi-steady state

Steady state conditions were reached on the order of ~10 simulated seconds Since the diffusion of volatiles was not accounted for, this time should not strictly be comparable to eruptive timescales.

3.2.1. Below the fragmentation level

All the simulations produced similar results in the portion of the conduit below the fragmentation level. The fragmentation process for centimeter size particles, especially when the granular viscosity was calculated, was less efficient in moving material away from the fragmentation zone, and hence magma lower in the conduit was at slightly elevated pressures. This inhibited exsolution and consequently resulted in slightly lower velocities (Figs. 5 and 6). There was little differential velocity ($\ll$1%) of bubbles and magma below the fragmentation level in any of the simulations. However, there was higher pressure in the center of the conduit, so that at any particular depth there was greater exsolution at the edges of the conduit. This process may have implications for gas loss from the conduit walls as was pointed out by Wilson (1998). Using an analytical calculation, Wilson demonstrated that the effect of increasing viscosity with height was sufficient to produce small lateral

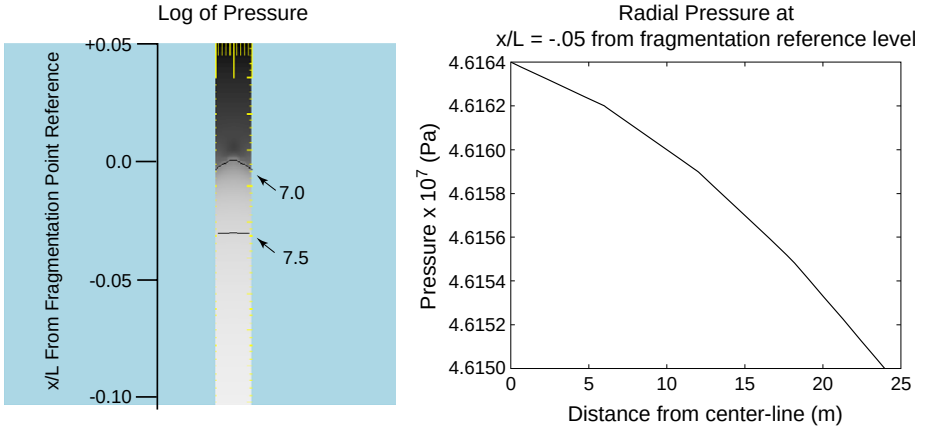

Fig. 7. Two-dimensional cross-section of pressure near fragmentation: Pressures are displayed on the left as log of Pa. The right panel shows the radial distribution of pressure from the center of the conduit to the edge of the conduit. Both illustrate the higher pressure in the center of the conduit.

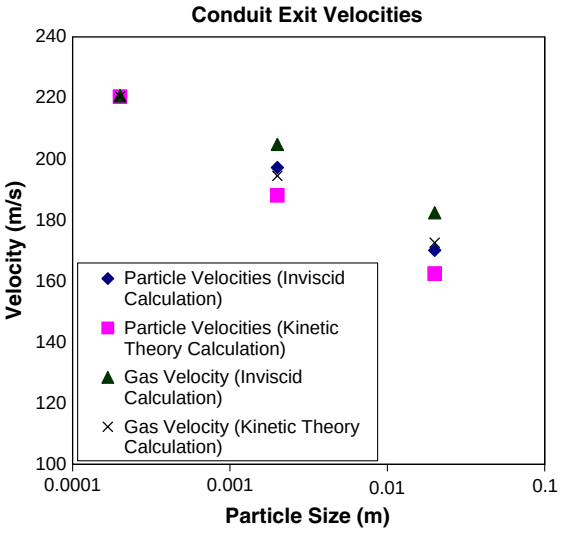

Fig. 8. Centerline conduit exit velocities: Gas and particle velocities are shown for .0002 m, .002 m, and .02 m particle calculations. Both the effective granular viscosity calculations and inviscid calculations are shown.

pressure variations in the conduit. This apparently is the same mechanism at work in the present calculations as the regions of the greatest vertical viscosity gradient (just below fragmentation) have the largest horizontal pressure gradients (Fig. 7). The vertical increase of viscosity with height is a result of volatile exsolution at lower pressure (Hess and Dingwell, 1996). In these calculations the horizontal pressure variation below fragmentation accounted for about a 3% drop from center-conduit to sidewall.

3.2.2. Above the fragmentation level

Fig. 8 shows the centerline conduit exit velocities for gas and particles during these simulations. Both the inviscid and granular viscosity calculations show that the relative gas–particle velocity increases with increasing particle size. The eruptions with .0002 m particles have particle and gas velocities that are virtually indistinguishable, whereas the .02 m particles, for the inviscid calculation, have center-line vertical velocities of 182.4 m/s and 170.1 m/s for the gas and particles, respectively.

The greater gas–particle differential velocity observed for the larger particles can be interpreted in terms of the aerodynamic response timescales of the different particles. The particle response times can be estimated from Eq. (2) and are 5.31×10^{-1} s for the .0002 m particles, 5.31×10^{-1} s for the .002 m particles and 5.31×10^{-1} s for the .02 m particles. Eq. (2) applies for smooth, spherical particles with small particle Reynolds numbers. The larger particles considered here, .002 m and .02 m, have significant differential gas–particle velocity and have particle Reynolds numbers in excess of 100 (Eq. (42)). Therefore, a more sophisticated approach is warranted to estimate their response timescales. An aerodynamic timescale can be developed from the drag relation used in this multi-fluid study (Syamlal formulation, Eq. (37)) that is based on terminal velocity correlations and accounts for the volume fraction of particles present. Neglecting the buoyancy term, this equation recast is:

$$\frac{m_{\mathrm{p}}\dfrac{\mathrm{d}\mathbf{u}_i^{\mathrm{s}}}{\mathrm{d}t}}{V} = \frac{3\varepsilon_{\mathrm{p}}\varepsilon_{\mathrm{g}}\rho_{\mathrm{g}}}{4V_{\mathrm{r}}^2 d_{\mathrm{p}}} C_{\mathrm{D}}^{\mathrm{s}}|\mathbf{u}_i^{\mathrm{g}} - \mathbf{u}_i^{\mathrm{p}}|(\mathbf{u}_i^{\mathrm{g}} - \mathbf{u}_i^{\mathrm{p}}), \qquad (43)$$

where m_{p} is the total mass of the solid phase in a control (V). Velocities in this equation are the fluid, or average velocities of the gas and particles. The macroscopic density of the particles (m_{p}/V) can be written in terms of the single particle density, ρ_{p} using the volume fraction of the particles in the

Table 2
Summary of particle timescales[a]

Particle size (m)	Average differential velocity (m/s)	Particle Reynolds number, Re_{p}	$C_{\mathrm{D}}^{\mathrm{w}}$	$C_{\mathrm{D}}^{\mathrm{s}}$	$C_{\mathrm{D}}^{\mathrm{s}}/V_{\mathrm{r}}^2$	Low Re aerodynamic timescale, t_{p} (s)	Wilson's formulation timescale, $t_{\mathrm{p}}^{\mathrm{w}}$ (s)	Syamlal's formulation timescale, $t_{\mathrm{p}}^{\mathrm{s}}$ (s)
.0002	.05	.25	96	70	166	.53	.55	.36
.002	2.5	125	1.22	.99	1.79	53	8.7	6.6
.02	6.0	300	1.22	.50	.87	5300	37	56

[a] Average differential velocity between the gas and solid phase is estimated as the difference in the centerline velocities at the conduit exit divided by 2. Calculation of $C_{\mathrm{D}}^{\mathrm{w}}$ is given by $24/Re_{\mathrm{p}}$ for Re_{p} <100 and 1.22 for higher Reynolds' number (Wilson, 1999).

control volume. Then rearrangement of the terms gives:

$$\frac{\mathrm{d}\mathbf{u}_i^{\mathrm{s}}}{\mathrm{d}t} = \frac{3\varepsilon_{\mathrm{g}}\rho_{\mathrm{g}}}{4V_{\mathrm{r}}^2 d_{\mathrm{p}}\rho_{\mathrm{p}}} C_{\mathrm{D}}^{\mathrm{s}} |\mathbf{u}_i^{\mathrm{g}} - \mathbf{u}_i^{\mathrm{s}}| \left(\mathbf{u}_i^{\mathrm{g}} - \mathbf{u}_i^{\mathrm{s}}\right), \tag{44}$$

and a timescale of:

$$t_{\mathrm{p}}^{\mathrm{s}} = \frac{4V_{\mathrm{r}}^2 d_{\mathrm{p}}\rho_{\mathrm{p}}}{3\varepsilon_{\mathrm{g}}\rho_{\mathrm{g}} C_{\mathrm{D}}^{\mathrm{s}} |\mathbf{u}_i^{\mathrm{g}} - \mathbf{u}_i^{\mathrm{s}}|}. \tag{45}$$

Assuming an average volume fraction of particles of 0.1 that is typical in these simulations, the corresponding timescale are .36 s, 6.6 s, and 56 s for .002 m, and .02 m particles, respectively (assumptions used in these calculations listed in Table 2). These timescale can be compared to the single-particle drag formulation of Wilson (1999) that considered particle roughness and yielded timescales of .56 s, 8.7 s, and 36 s, respectively.

$$t_{\mathrm{p}}^{\mathrm{w}} = \frac{4d_{\mathrm{p}}\rho_{\mathrm{s}}}{3\rho_{\mathrm{g}} C_{\mathrm{D}}^{\mathrm{w}} |\mathbf{u}_i^{\mathrm{g}} - \mathbf{u}_i^{\mathrm{s}}|} \tag{46}$$

The Wilson relation (Eq. (46)) and the Syamlal relation (Eq. (45)) are equivalent in form for dilute conditions

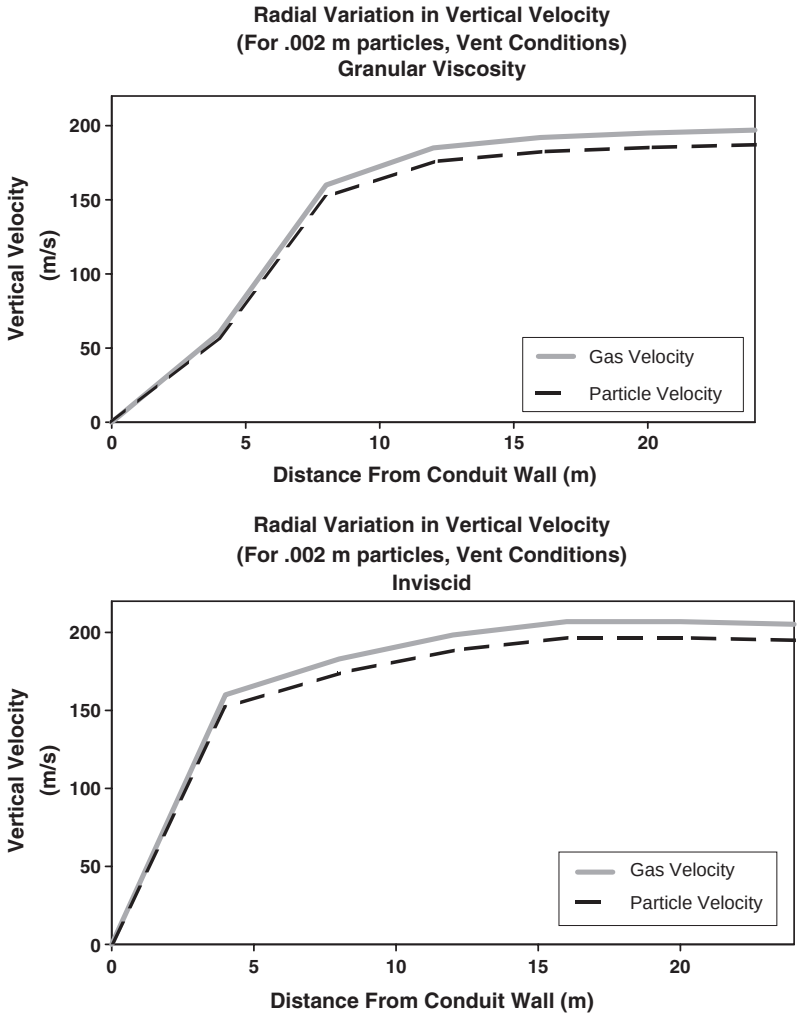

Fig. 9. Radial variation in the vertical velocity at the vent: Velocity of the gas (—) and particles (- - -) are shown for the granular viscosity (top) and inviscid (bottom) calculations using .002 m particles. In both cases the gas exits the conduit with greater velocity, and the relative velocity is greatest in the center of the conduit. In the annular or near-wall region, the velocity of both phases decreases more rapidly further from the wall in the granular viscosity calculation.

($\varepsilon_g \rightarrow 1.0$) and if $C_D^w = C_D^s / V_r^2$. The formulation for these timescales and particle Reynolds number is summarized in Table 2. The drag correlation developed by Syamlal was used in this study, and hence these timescales are of the most relevance in interpreting our results, although qualitatively any of the drag formulations would have produced differential particle–gas velocities for the .02 m particles for this conduit geometry. Assuming an average transit time on the order of 10 s from fragmentation to conduit exit gives equivalent Stokes numbers of approximately .036, .66, and 5.59 for .0002 m, .002 m, and .02 m particles, respectively. Only the .0002 m particles have sufficient time to respond completely to the gas velocity by the conduit exit.

One key finding from our work is that including the granular viscosity calculation decreases the velocities of the particle and gas phases in simulations with particles greater than about a millimeter. At the conduit exit, this results in centerline velocities of 172.6 m/s for the gas phase and 162.5 m/s for the particle phase when .02 m particles are considered. Again, the calculation with .0002 m particles shows little difference in velocities when the granular stress is considered. It should be noted that the constitutive equations for the gas phase remained the same during all of the simulations. When collisions produced a granular viscosity, the particle phase was slowed, created a greater magnitude drag force between the gas and the particles, and, as a result, slowed the gas. Figs. 5 and 6 show the centerline vertical velocities of the gas and particles in the near fragmentation area. Immediately following fragmentation the particle phase with the granular viscosity is slowed compared to the inviscid particle phase for even the .0002 m particles. However, as the conduit exit is reached the velocity difference is diminished for the .0002 m particles. For both the .002 m and .02 m particle sizes the viscous particle phase remains slower than its inviscid counterpart from the point of fragmentation to the conduit exit.

The centerline velocities are the maximum velocities in the conduit for both the inviscid and granular viscosity calculations. However, the radial velocity profile at the vent of the conduit varies with the assumption used for the granular stress. For example, Fig. 9 shows the velocities at the vent for the .002 m particles for both the inviscid and granular viscosity cases. In general, the velocities are greater in the inviscid case, and decrease less rapidly in the annular flow region than do the velocities in the granular viscosity case. This has a subtle effect on the mass-flux calculations given in Table 1, and results in greater flux of material for the inviscid calculations. In many industrial riser flows a negative annular velocity is often detected (Miller and Gidaspow, 1992; Neri and Gidaspow, 2000) which is not observed here. However, in the experiments reported by Miller and Gidaspow (1992) the negative velocity disappears for large magnitude vertical velocities. Another mitigating factor is the use of no-slip boundary conditions for the gas and particle phase; one avenue of future research will be to examine the effect of partial slip boundaries on the particle phase (Neri and Gidaspow, 2000).

The spatial distribution of the volume fraction of gas is also changed as a result of modifying the particle size. The larger particles diminish the vertical gradient of volume fraction of gas (Fig. 10) so that fragmentation occurs at a higher level in

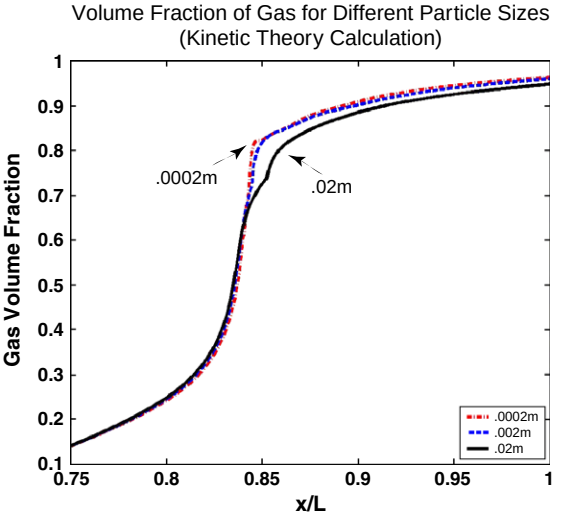

Fig. 10. Volume fraction of gas for different particle sizes: Conduit height is non-dimensionalized by the length of the conduit and is referenced from the bottom of the conduit (8 km). The larger particles decrease the gradient of volume fraction near fragmentation (.75). A larger volume fraction of the centimeter-scale particles exits the conduit.

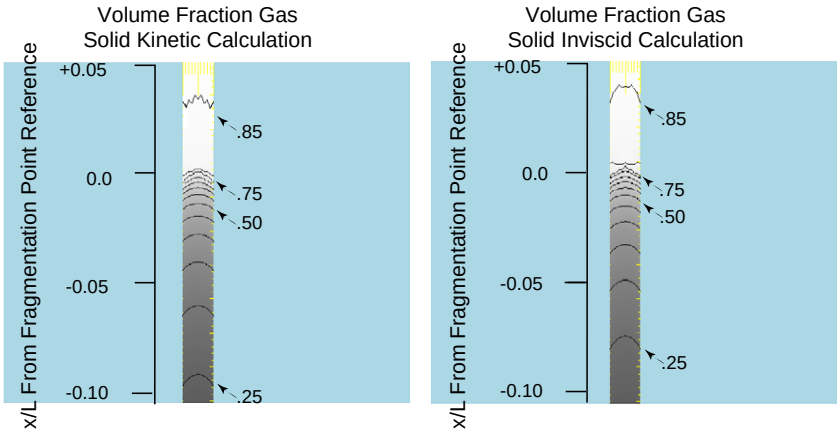

Fig. 11. Two-dimensional cross-section of gas volume fraction near fragmentation: The granular viscosity (kinetic theory calculation) and the inviscid calculation volume fractions are shown for .002 m particles. The particle volume fraction above fragmentation is slightly more focused in the granular viscosity calculation than in the inviscid calculation.

the conduit for the larger particle sizes. As a result, a greater volume fraction of particles leaves the conduit exit when larger particles are considered, although with a lower velocity. The granular viscosity calculation lowers the vertical gradients in the volume fraction of gas in the near fragmentation zone as is depicted in Fig. 11. The calculation of granular stress also increases the near wall concentration of particles compared to the inviscid simulations (Fig. 12). This result is consistent with the observation of core-annular granular flow in industrial risers (Miller and Gidaspow, 1992).

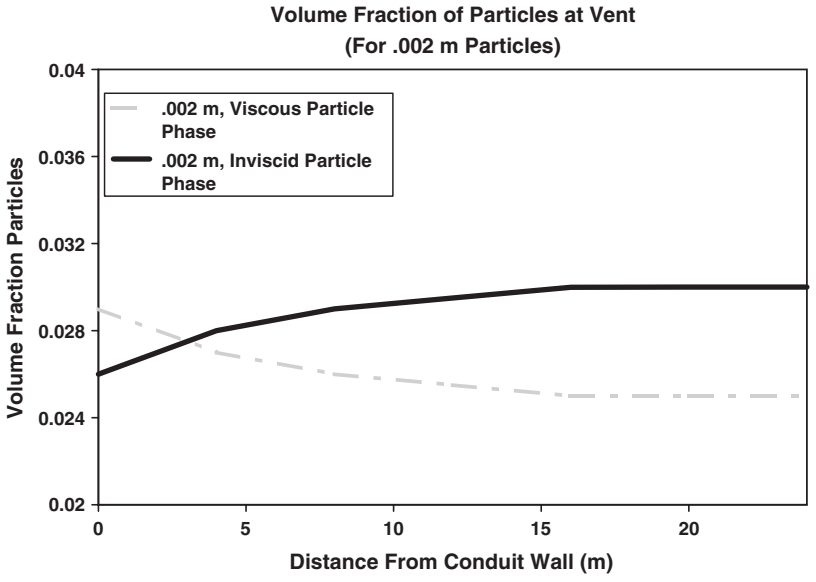

Fig. 12. Radial variation in the particle volume fraction at the vent: The volume fraction for the granular viscosity (grey line) and inviscid (black line) calculation for .002 m are compared. The calculations using granular viscosity show slightly greater volume fraction in the near-wall region than in the center-conduit.

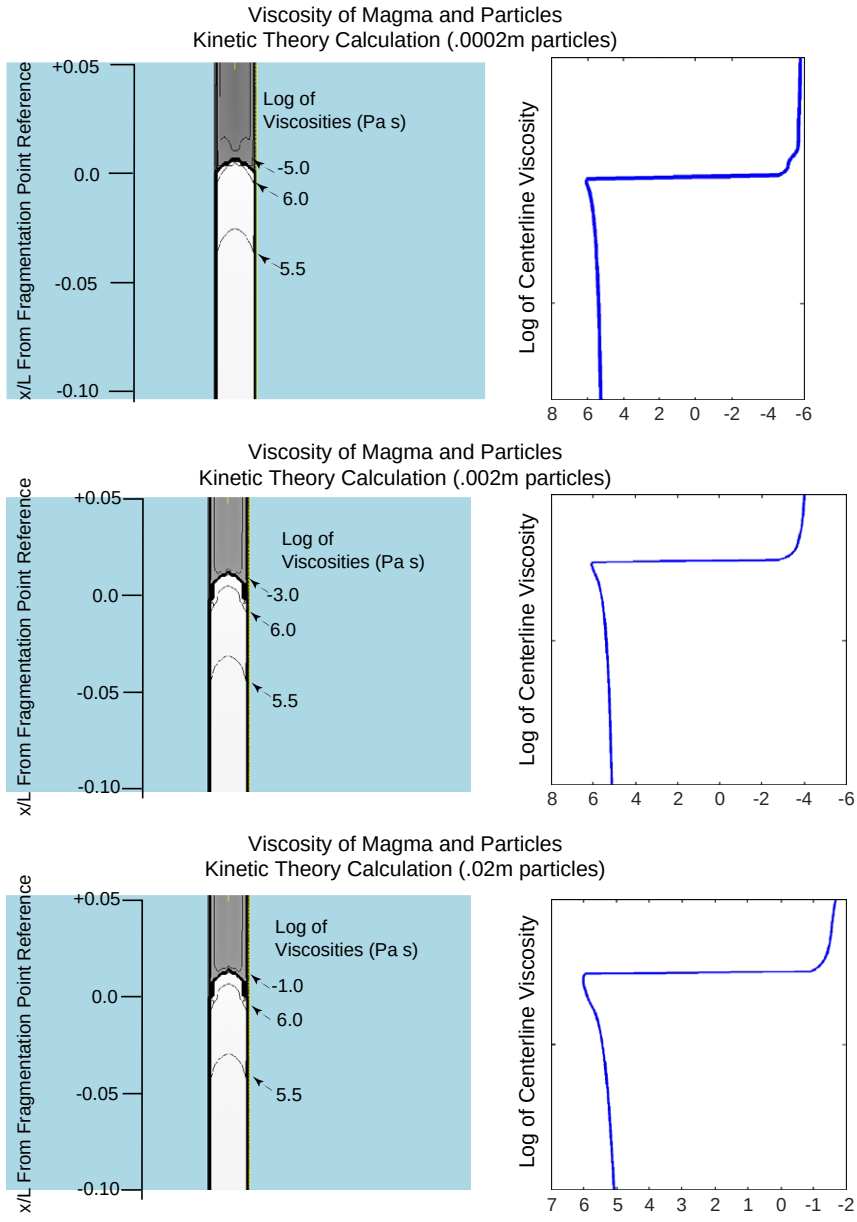

Fig. 13. Granular viscosity following fragmentation: Effective granular viscosity calculations are shown corresponding to the three particle sizes .0002 m, .002 m, and .02 m. Viscosity is given as the log of Pa · s.

The viscosities that result from the kinetic theory calculation are depicted in Fig. 13. The sub-millimeter particles have viscosities after fragmentation that are approximately 10^{-5} Pa · s which is very near to the viscosity of a gas phase at these elevated temperatures. However, the .02 m particles produce viscosities after fragmentation of about 10^{-1} Pa · s. The granular viscosity is highest immediately following fragmentation and also near to the side-wall boundaries. This is primarily a result of the

slightly higher volume fraction of particles in these regions. Examination of Eqs. (26) and (28) shows that as the volume fraction of particles goes to zero, the granular viscosity must also go to zero. The correlation of volume fraction to granular viscosity has also been noted in the riser experiments (Miller and Gidaspow, 1992). Modifying the coefficient of restitution from .8 to .5 changed the granular viscosity to ~15% lower values.

4. Conclusions

The results from this parametric study of the granular stress in the context of a rhyolitic conduit eruption show that the inclusion of a granular viscosity calculation is probably not necessary for particles of the order .0002 m or smaller. These sub-millimeter particles have granular viscosities on the order of 10^{-5} Pa·s in the conduit setting. However, .002 m and .02 m particles have ~5% differences in the particle centerline velocity and maximum granular viscosities of the order of 10^{-3} Pa·s and 10^{-1} Pa·s, respectively, when collisions are considered.

The use of a two-dimensional model permitted the calculation of radial variations in volume fraction and velocity of gas and particles exiting the conduit. The granular viscosity calculation predicted a greater volume fraction of particles in the near-wall region at the conduit vent than did the inviscid calculation. The velocities at the vent for the inviscid calculations were in general higher than the granular viscosity calculations, and had a larger gradient $\left(\frac{\partial v}{\partial x}\right)$ in the near-wall region. Two-dimensional conduit models, such as the one used in this study, may be implemented in the future to determine the structure of more complex flows, evaluate the speed of mixtures of gas/particles for irregular vent geometries, and to evaluate phase distribution in conduits. To extend this approach several aspects of the numerical modeling deserve closer inspection including grid refinement, lack of an imposed symmetry axis or fully three-dimensional simulations, use of a turbulence model, and exploration of partial slip boundaries for conduit flow.

The majority of previous conduit models have used smaller particles as part of the complete atomization assumption (Papale, 2001). That is, magmatic foam is assumed to be completely destroyed in the fragmentation process. The grain size distributions of many volcanic eruptions, however, have abundant pumice clasts much larger than the .0002 m limit (Bachmann et al., 2000; Bursik, 1998). Papale (2001) demonstrated that this inefficient fragmentation could significantly alter conduit exit conditions by lowering velocities and pressures. The results of this parametric study show that inefficient fragmentation may also produce larger pumices that are significantly slowed through particle–particle interaction as well as having a larger aerodynamic response time (Burgisser and Bergantz, 2002; Eaton and Fessler, 1994). The viscous particle phase will slow both phases relative to an inviscid calculation. Future conduit modeling efforts may include modeling multiple sizes fractions of pumices in a multi-fluid effort similar to the work of Neri et al. (2002) for pyroclastic flows. This study suggests that the size fractions greater than a millimeter will produce at least a ~5% change in the vertical centerline velocity, and up to ~10% change in the average vertical velocity if particle collisions are considered. The lower velocities may then modify the eruptive behavior of the conduit system by altering velocities and pressure of the different phases through particle–particle and particle–gas interaction.

Acknowledgements

This research has been supported by a DoD National Defense Science and Engineering Graduate Fellowship (JD) and NSF Grant EAR-9805336 (GWB). Correspondence with M. Syamlal and S. Dartevelle aided the development of the numerical aspects of this study and is greatly appreciated. Encouragement and discussions with P. Papale, A. Neri, and A. Clarke are warmly acknowledged. Thoughtful reviews by L. Wilson, O. Melnik, and S. Dartevelle were very useful in the preparation of this manuscript. We thank D. Sahagian and A. Proussevitch for organizing and NSF for sponsoring the Volcanic Eruption Mechanism Modeling Workshop (2002).

Appendix A

Notation

$\mathbf{c}_I$	Instantaneous velocity (m/s)
$\mathbf{C}_I$	Fluctuating velocity (m/s)
C_{eq}	Equilibrium solubility of water (wt.%)
C_D^s	Particle drag function (Syamlal)
C_D^w	Particle drag function (Wilson)
$\mathbf{D}_{ij}$	Strain rate tensor (s^{-1})
d_p	Particle diameter (m)
d_{bub}	Bubble diameter (m)
e	Coefficient of restitution
f	Velocity frequency distribution
f_{coll}	Frequency distribution of particle collisions
$\mathbf{g}$	Gravitational acceleration (m/s^2)
g_0	Radial distribution function
$\mathbf{I}_i$	Inter-phase drag (N/m^3)
l	Mean free path (m)
m_p	Mass of particle (kg)
M	Momentum Flux ($kg \cdot m/s^1$)
P	Pressure (Pa)
R	Exsolution rate ($kg/m^3 \cdot s$)
Re_p	Particle Reynolds number
$\mathbf{S}_{ij}$	Stress tensor (Pa)
t_p	Particle timescale (s)
T	Temperature (K)
$\mathbf{u}_i$	Average velocity (m/s)
V_r	Ratio of the terminal velocity of a group of particles to a single particle
ΔV_g	Volume fraction of water exsolved during one time-step (kg/m^3 s)
Δt	Time-step (s)
ε	Volume fraction
δ_{ij}	Kronecker delta
λ	Second viscosity coefficient ($Pa \cdot s$)
ξ	Bulk viscosity ($Pa \cdot s$)
μ	Shear viscosity ($Pa \cdot s$)
θp	Granular temperature (m^2/s^2)
ρ	Density (kg/m^3)
$\boldsymbol{\tau}_{ij}$	Deviatoric stress tensor (Pa)

Subscripts

g	Gas phase
m	Magma
p	Particles
gp	Gas–particle interaction
gm	Gas–magma interaction
$\langle\rangle$	Average

Appendix B

As shown by Chapman and Cowling (1952) a general transport equation for a quantity γ is:

$$\frac{\partial n\langle\gamma\rangle}{\partial t} + \frac{\partial}{\partial \mathbf{x}_j} n\langle\gamma c_i\rangle - n\mathbf{F}_i\left\langle\frac{\partial \gamma}{\partial \mathbf{c}_i}\right\rangle = \int \gamma\left(\frac{\partial f}{\partial t}\right)_{coll} d\mathbf{c}_i \quad (a)$$

where f is the frequency distribution of velocities, $\mathbf{F}_i$ is specific-force (N/kg), n is the number of particles in a control volume, $\left(\frac{\partial f}{\partial t}\right)_{coll}$ is the rate of change of the frequency distribution of particles as a result of collisions, and the average for a quantity is defined as:

$$n\langle\gamma\rangle = \int \gamma f \, d\mathbf{c}_i. \quad (b)$$

If no collisions occur, the source term on the right hand side of Eq. (a) goes to zero. To obtain an equation for the transport of momentum, let $\gamma = m\mathbf{c}_j$, where m is the mass of a particle. Using the fact that the product of the mass and number of particles is equal to the product of the density and volume fraction of particles ($m_p n = \rho_p \varepsilon_p$) and decomposing the velocity, $\mathbf{c}_j$, into its fluctuating component, $\mathbf{C}_j$, and its average $\mathbf{u}_j$ gives:

$$\frac{\partial \rho\varepsilon\mathbf{u}_j}{\partial t} + \frac{\partial}{\partial \mathbf{x}_i}\rho\varepsilon\mathbf{u}_i\mathbf{u}_j + \frac{\partial}{\partial \mathbf{x}_i}\rho\varepsilon\langle\mathbf{C}_i\mathbf{C}_j\rangle - \rho\varepsilon\mathbf{F}_i\mathbf{d}_{ij} = 0. \quad (c)$$

To obtain this result note that:

$$\begin{aligned}\big\langle(\langle\mathbf{c}_i\rangle + \mathbf{C}_i)(\langle\mathbf{c}_j\rangle + \mathbf{C}_j)\big\rangle &= \langle\mathbf{u}_i\mathbf{u}_j + \mathbf{C}_i\mathbf{u}_j + \mathbf{C}_j\mathbf{u}_i + \mathbf{C}_i\mathbf{C}_j\rangle \\ &= \mathbf{u}_i\mathbf{u}_j + \langle\mathbf{C}_i\mathbf{C}_j\rangle, \quad (d)\end{aligned}$$

$$\frac{\partial \mathbf{u}_j}{\partial \mathbf{u}_i} = l \quad \text{if } i = j, \quad (e)$$

and

$$\frac{\partial \mathbf{u}_j}{\partial \mathbf{u}_i} = 0 \quad \text{if } i \neq j. \quad (f)$$

A common first approximation of granular flows (Gidaspow, 1994; Chapman and Cowling, 1952) is that the velocity varies randomly about the mean velocity (i.e. it has a Maxwellian velocity distribution). Hence,

it can be shown that the off diagonal terms of the $\langle \mathbf{C}_i \mathbf{C}_j \rangle$ tensor go to zero leaving the equation:

$$\frac{\partial \rho_p \varepsilon_p \mathbf{u}_j}{\partial t} \frac{\partial}{\partial \mathbf{x}_i} \rho_p \varepsilon_p \mathbf{u}_i \mathbf{u}_j + \frac{\partial}{\partial \mathbf{x}_i} \rho_p \varepsilon_p \langle \mathbf{C}_i \mathbf{C}_j \rangle \boldsymbol{\delta}_{ij} - \rho_p \varepsilon_p \mathbf{F}_i \boldsymbol{\delta}_{ij} = 0, \quad \text{(g)}$$

where the term $\rho_p \varepsilon_p \langle \mathbf{C}_i \mathbf{C}_j \rangle \boldsymbol{\delta}_{ij}$ acts as the kinetic, or translational, stress in the equation. Eq. (g) is the equation of an inviscid granular material, and thus a good approximation is that a collision-less granular material is inviscid (Gidaspow, 1994).

References

Agrawal, K., Loezos, P.N., Syamlal, M., Sundaresan, S., 2001. The role of meso-scale structures in rapid gas–solid flows. Journal of Fluid Mechanics 445, 151–185.

Anderson Jr., A.T., Newman, S., Williams, S.N., Druitt, T.H., Skirius, C., Stolper, E., 1989. H_2O, CO_2, Cl and gas in Plinian and ash-flow Bishop rhyolite. Geology 17, 221–225.

Bachmann, O., Dungan, M.A., Lipmann, P.W., 2000. Voluminous lava-like precursor to a major ash-flow tuff: low-column pyroclastic eruption of the Pagosa Peak Dacite, San Juan volcanic field, Colorado. Journal of Volcanology and Geothermal Research 98, 153–171.

Burgisser, A., Bergantz, G.W., 2002. Reconciling pyroclastic flow and surge: the multiphase physics of pyroclastic density currents. Earth and Planetary Science Letters 202, 405–418.

Bursik, M., 1998. Tephra dispersal. In: Gilbert, J.S., Sparks, R.S.J. (Eds.), The Physics of Explosive Volcanic Eruptions. Geological Society Special Publication, London, UK, pp. 115–144.

Carey, S., Sigurdsson, H., 1989. The intensity of Plinian eruptions. Bulletin of Volcanology 51, 28–40.

Chapman, S., Cowling, T.G., 1952. The Mathematical Theory of Non-Uniform Gases; an Account of the Kinetic Theory of Viscosity, Thermal Conduction, and Diffusion in Gases. Cambridge University Press.

Dingwell, D.B., 1996. Volcanic dilemma: flow or blow? Science 273, 1054–1055.

Dobran, F., 1992. Nonequilibrium flow in volcanic conduits and application to the eruptions of Mt. St. Helens on May 18, 1980, and Vesuvius in AD 79. Journal of Volcanology and Geothermal Research 49, 285–311.

Dobran, F., 1993. Global Volcanic Simulation of Vesuvius. Giardini. 148 pp.

Dobran, F., 2001. Volcanic Processes, Mechanisms in Material Transport. Kluwer Academic. 590 pp.

Dobran, F., Neri, A., Macedonio, G., 1993. Numerical simulation of collapsing volcanic columns. Journal of Geophysical Research 98, 4231–4259.

Eaton, J.K., Fessler, J.R., 1994. Preferential concentration of particles in turbulence. International Journal of Multiphase Flow 20, 169–209 (Suppl.).

Gardner, J.E., Thomas, R.M.E., Jaupart, C., Tait, S., 1996. Fragmentation of magma during Plinian volcanic eruptions. Bulletin of Volcanology 58, 144–162.

Gidaspow, D., 1986. Hydrodynamics of fluidization and heat transfer: supercomputer modeling. Applied Mechanics Reviews 39, 1–23.

Gidaspow, D., 1994. Multiphase Flow and Fluidization: Continuum and Kinetic Theory Descriptions. Academic Press. 467 pp.

Harlow, F.H., Amsden, A.A., 1975. Numerical calculation of multiphase flow. Journal of Computational Physics 17, 19–52.

Hess, K.U., Dingwell, D.B., 1996. Viscosities of hydrous leucogranitic melts: a non Arrhenian model. American Mineralogist 81, 1297–1300.

Hurwitz, S., Navon, O., 1994. Bubble nucleation in rhyolitic melts: experiments at high pressure, temperature and water content. Earth and Planetary Science Letters 122, 267–280.

Jackson, R., 1983. Some mathematical and physical aspects of continuum models for the motion of granular materials. In: Meyer, R.E. (Ed.), Theory of Dispersed Multiphase Flow. Academic Press, Inc, New York, NY.

Johnson, K.L., 1985. Contact Mechanics. Cambridge University Press, Cambridge, UK.

Lebowitz, J.L., 1964. Exact solution of generalized Percus–Yevick equation for mixture of hard spheres. Physical Review. A 133, 895–899.

Lun, C.K.K., Savage, S.B., Jeffrey, D.J., Chepuniy, N., 1984. Kinetic theories for granular flow: inelastic particles in Couette flow and slighty inelastic particles in a general flow field. Journal of Fluid Mechanics 140, 223–256.

Lyakhovsky, V., Hurwitz, S., Navon, O., 1996. Bubble growth in rhyolitic melts: experimental and numerical investigation. Bulletin of Volcanology 58, 19–32.

Mader, H.M., 1998. Conduit flow and fragmentation. In: Gilbert, J.S., Sparks, R.S.J. (Eds.), The Physics of Explosive Volcanic Eruptions. Geological society special publication, London, UK, pp. 51–70.

Maxey, M.R., Riley, J.J., 1983. Equation of motion for a small rigid sphere in non uniform flow. Physics of Fluids 26, 883–889.

Melnik, O.E., Barmin, A.A., Sparks, R.S.J., 2003. Conduit flow model for the case of high-viscous, gas-saturated magma. Journal of Volcanology and Geothermal Research (this volume).

Miller, A., Gidaspow, D., 1992. Dense, vertical gas–solid flow in a pipe. American Institute of Chemical Engineers Journal 38, 1801–1815.

Neri, A., Gidaspow, D., 2000. Riser hydrodynamics: simulation using kinetic theory. Particle Technology and Fluidization 46, 52–67.

Neri, A., Macedonio, G., 1996. Numerical simulation of collapsing volcanic columns with particles of two sizes. Journal of Geophysical Research 101, 8153–8174.

Neri, A., Di Muro, A., Rosi, M., 2002. Mass partition during collapsing and transitional columns by using numerical simulations. Journal of Volcanology and Geothermal Research 115, 1–18.

O'Brien, T.J., Syamlal, M., 1991. Fossil fuel circulating fluidized bed: simulation and experiment. In: Gaden, E.L., Weimer, A.W.

(Eds.), Advances in Fluidized Systems. American Institute of Chemical Engineers Symposium Series, pp. 127–136.

Papale, P., 1999. Strain-induced magma fragmentation in explosive eruptions. Nature 397, 425–428.

Papale, P., 2001. Dynamics of magma flow in volcanic conduits with variable fragmentation efficiency and nonequilibrium pumice degassing. Journal of Geophysical Research 106, 11043–11065.

Papale, P., Dobran, F., 1994. Magma flow along the volcanic conduit during the Plinian and pyroclastic flow phases of the May 18, 1980, Mt. St. Helens eruption. Journal of Geophysical Research 99, 4355–4373.

Papale, P., Polacci, M., 1999. Role of carbon dioxide in the dynamics of magma ascent in explosive eruptions. Bulletin of Volcanology 60, 583–594.

Papale, P., Neri, A., Macedonio, G., 1998. The role of magma composition and water content in explosive eruptions—1. Conduit ascent dynamics. Journal of Volcanology and Geothermal Research 87, 75–93.

Slezin, Y.B., 2003. The mechanism of volcanic eruptions (a steady state approach). Journal of Volcanology and Geothermal Research 122, 7–50.

Sparks, R.S.J., 1978. Dynamics of bubble formation and growth in magmas—review and analysis. Journal of Volcanology and Geothermal Research 3, 1–37.

Syamlal, M., 1987. A review of granular stress constitutive relations. Technical Report: DOE/MC/21353-2372. Department of Energy, Springfield, VA.

Syamlal, M., Rogers, W., O'Brien, T.J., 1993. MFIX Documentation: Theory Guide. DOE/METC-94/1004. U.S. Department of Energy, Morgantown, WV.

Thomas, N., Jaupart, C., Vergniolle, S., 1994. On the vesicularity of pumice. Journal of Geophysical Research 99, 15633–15644.

Wilson, S.D.R., 1998. A mechanism for the lateral transport of gas bubbles in silicic lava rising in a vertical conduit. Earth and Planetary Science Letters 256, 13–18.

Wilson, L., 1999. Explosive volcanic eruptions—X. The influence of pyroclast size distributions and released magma gas contents on the eruption velocities of pyroclasts and gas in Hawaiian and Plinian eruptions. Geophysical Journal International 136, 609–619.

Wilson, J., Head III, J.W., 1981. Ascent and eruption of basaltic magma on the earth and the moon. Journal of Geophysical Research 86, 2971–3001.

Zhang, Y.X., 1999. Exsolution enthalpy of water from silicate liquids. Journal of Volcanology and Geothermal Research 88, 201–207.